

Strong-coupling superconductivity in the kagome metal CsV_3Sb_5 revealed by soft point-contact spectroscopy

Ming-chong He (何明冲)¹, Hai Zi (子海)¹, Hong-xing Zhan (詹红星)¹, Yu-qing Zhao (赵宇清)¹, Cong Ren (任聪)^{1,*}, Xing-yuan Hou (侯兴元)², Lei Shan (单磊)², Qiang-hua Wang (王强华)^{3,†}, Qiangwei Yin (殷蔷薇)⁴, Zhijun Tu (涂志俊)⁴, Chunsheng Gong (龚春生)⁴, Hechang Lei (雷和畅)⁴, Zhong-yi Lu (卢仲毅)⁴, Qi Wang (王琦)^{5,6}, Yan-peng Qi (齐彦鹏)^{5,6}, Gen-fu Chen (陈根富)⁷ and Peng Xiong⁸

¹*School of Physics and Astronomy, Yunnan University, Kunming 650500, China*

²*Information Materials and Intelligent Sensing Laboratory of Anhui Province, Institutes of Physical Science and Information Technology, Anhui University, Hefei 230601, China*

³*School of Physics, Nanjing University, Nanjing 210093, China*

⁴*Department of Physics and Beijing Key Laboratory of Opto-electronic Functional Materials and Micro-nano Devices, Renmin University of China, Beijing 100872, China*

⁵*School of Physical Science and Technology, ShanghaiTech University, Shanghai 201210, China*

⁶*ShanghaiTech Laboratory for Topological Physics, ShanghaiTech University, Shanghai 201210, China*

⁷*Beijing National Laboratory for Condensed Matter Physics, Institute of Physics, CAS, Beijing 100190, China*

⁸*Department of Physics, Florida State University, Tallahassee, Florida 32306 USA*



(Received 17 April 2022; revised 4 August 2022; accepted 31 August 2022; published 16 September 2022)

The nature of the superconducting state in kagome metals AV_3Sb_5 is a key issue in need of experimental clarification. Here, we report on a study of the superconducting order parameter in the kagome superconductor CsV_3Sb_5 through simultaneous “soft” point-contact spectroscopy and resistivity measurements under both ambient and a hydrostatic pressure. Signatures of two-gap superconductivity are resolved in the soft point-contact spectra, accompanied by an asymmetric excess conductance above T_c . Quantitative analysis based on the two-dimensional Blonder-Tinkham-Klapwijk model reveals an $(s + s)$ -wave superconducting gap with $2\Delta_0/k_B T_c \simeq 7.2$, placing CsV_3Sb_5 in the strong-coupling regime. The strong-coupling two-gap feature indicates a high electronic density of states (DOS) and possible existence of flat-band-driven multiple van Hove singularities (VHSs) at the Fermi level. The presence of asymmetric excess spectral conductance above T_c hints at a modest electronic correlation in CsV_3Sb_5 . Under a hydrostatic pressure of 2.1 kbar, the nodeless multigap nature of the superconducting state remains, whereas both the larger gap and the excess spectral conductance are greatly suppressed, accompanied by an enhanced T_c . An estimate of the spectral-weighted gap ratio reveals a weakened coupling strength, indicative of a reduced total superconducting DOS upon pressure. Our results point to key roles of both flat-band-associated VHSs and electronic correlation in the onset of kagome superconductivity and shed some light on the interplay between charge-density-wave order and superconductivity in vanadium-based kagome superconductors.

DOI: [10.1103/PhysRevB.106.104510](https://doi.org/10.1103/PhysRevB.106.104510)

I. INTRODUCTION

The kagome lattice, consisting of a two-dimensional lattice of corner-sharing triangles, has become a paradigmatic setting for exotic quantum phenomena of electronic matter. Indeed, depending on the electron filling, on-site repulsion, and nearest-neighbor Coulomb interaction, the ground state of a kagome lattice system can be a quantum spin liquid [1–3], charge bond order [4,5], charge density wave (CDW) [6–8], or spin density wave [9]. Intriguingly, the recently discovered superconductivity in vanadium-based kagome metals, AV_3Sb_5 ($A = \text{K}, \text{Rb}, \text{Cs}$) adds a new physical dimension of electronic order to this novel system [10–12], making the family an ideal

playground to explore the correlation among superconductivity, CDW, and nontrivial band topology [13–15].

Concerning the physical origin of superconductivity in kagome metals AV_3Sb_5 , theoretical considerations have ruled out the possibility of a conventional electron-phonon coupling mechanism [16,17]. Despite the absence of long-range magnetic order or localized magnetic moments, the possible existence of magnetic fluctuations [10,18] was invoked as a potential pathway to unconventional superconductivity with a strong-coupling sublattice interference mechanism due to proximity to the flat-band-associated multiple van Hove singularities (VHSs) at the Fermi level [17,19–21]. On the experimental side, a distinct superconducting double dome is found to coexist with an intriguing CDW state in the temperature (T)–pressure (p) phase diagrams of AV_3Sb_5 , reminiscent of established unconventional superconductors (SCs) [22–24]. Signatures of unconventional superconductivity such as

*cren@ynu.edu.cn

†qhwang@nju.edu.cn

spin-triplet pairing were reported in $K_{1-x}V_3Sb_5$ -based Josephson junctions [25]. However, as for the specific gap structure and superconducting coupling strength, different experimental probes have produced disparate results. Thermal conductivity measurement appeared to suggest a nodal superconducting gap [26]. On the other hand, nuclear magnetic resonance experiments indicated a nodeless s -wave superconductivity competing with a unique CDW state [27,28]. Penetration depth along with specific heat measurements collectively point to two nodeless gaps in the weak-coupling limit in CsV_3Sb_5 [29], whereas low- T scanning tunneling microscopy (STM) appeared to show both nodal and nodeless sign-preserving gaps with multiple Fermi surfaces for the same material [30]. In addition, the different experimental probes are known to have varied sensitivities to different aspects of the band and spatial structures (e.g., surface versus bulk). It is apparent that the strong-coupling mechanism for kagome superconductivity has not been definitively established experimentally.

In this work, we performed point contact spectroscopy (PCS) measurements on single-crystalline CsV_3Sb_5 to investigate its state of superconducting pairing. From T dependence of the zero-bias conductance and analyses of the differential conductance curves $G(V)$ with the modified two-dimensional (2D) Blonder-Tinkham-Klapwijk (BTK) model, we obtain the gap size and superconducting transition temperature T_c^A on the same sample, resulting in reliable determination of the coupling strength for CsV_3Sb_5 . Our results highlight the importance of flat-band-associated van Hove singularities in the pairing state of kagome superconductivity.

II. EXPERIMENTAL DETAILS

Single crystals of CsV_3Sb_5 were synthesized using the self-flux method, in two different laboratories whose crystals are labeled as A and B. The crystal structure of CsV_3Sb_5 is depicted in Fig. 1(a). Figure 1(b) displays the x -ray diffraction pattern of a CsV_3Sb_5 single crystal. Only $(00l)$ diffraction peaks can be detected, indicative of the good crystalline nature of the single crystal [31]. Shown in the main panel of Fig. 1(c) is the ab -plane electrical resistivity $\rho_{xx}(T)$ in the entire temperature range with the residual resistance ratio $RRR \equiv R(300\text{ K})/R(5\text{ K})$ of 16 and 19 for samples A and B, respectively; a resistivity anomaly around 92 K is apparent and is ascribed to a CDW-like first-order phase transition. Meanwhile, ab -plane resistivity ρ_{xx} in the superconducting transition region is displayed in the inset of Fig. 1(c), showing bulk superconductivity with the onset superconductivity transition temperature T_c^{onset} and the zero resistivity temperature T_c^{zero} around 3.4 K and 2.5 K for both samples, respectively.

Andreev reflection spectroscopy (ARS) has been utilized to probe the nature of the superconducting gap in many SCs, including the two-gap MgB_2 [32], topological superconductors $Cu_xBi_2Se_3$ [33], $PbTaSe_2$ [34,35], and iron-based pnictides [36,37]. The measurement of ARS can be implemented either with a metal-tip point contact or soft planar contact geometry. Specifically, the soft planar point contacts have the advantage of avoiding inhomogeneous pressure or local strain effects induced by the metal tip, providing a pressureless spectroscopy measurement [38,39]. ‘‘Soft’’ planar contacts to the flat and

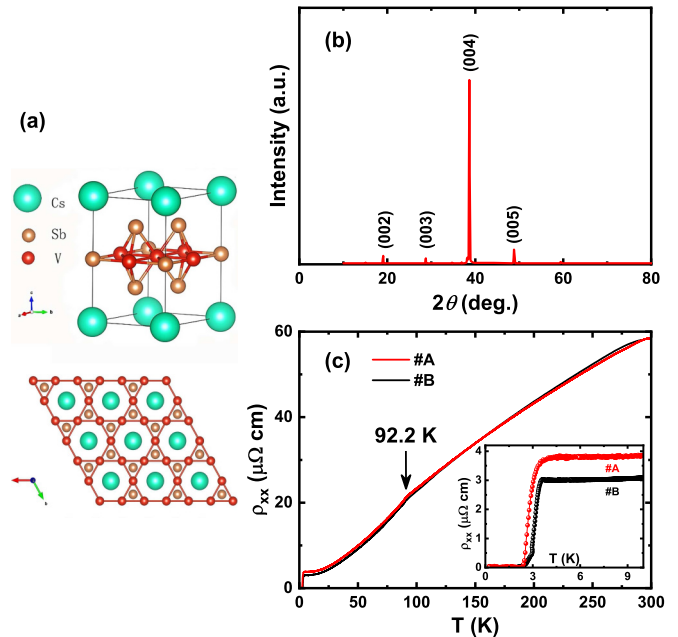


FIG. 1. (a) Crystal structure of CsV_3Sb_5 and an illustration of a top view of the lattice. The vanadium sublattice forms a perfect kagome lattice. (b) X-ray diffraction pattern of a typical CsV_3Sb_5 single crystal with the corresponding Miller indices $(00l)$. (c) Temperature dependence of resistivity $\rho_{xx}(T)$ for two pieces of CsV_3Sb_5 crystals. The arrow marks the resistivity anomaly at the charge-density-wave transition. Inset: The resistivity in the superconducting transition regime.

shiny surface cleaved along the c axis of CsV_3Sb_5 crystals were made using a thick silver paste bonding with platinum wires in a glove box. The typical size of these planar contacts is about 50–100 μm under a microscope. The heterocontact is actually composed of many nanocontacts due to the nanocrystalline nature of the silver paint, analogous to the tip point-contact technique. The differential conductance spectra were recorded with the standard phase-sensitive lock-in technique in a quasi-four-terminal configuration, where an AC modulation was applied to the sample on top of a DC current bias. The contact resistance R_J between the silver particles and CsV_3Sb_5 sample was usually in the range of 0.5–10 Ω , typical values of a genuine point contact between normal metals and superconductors.

III. RESULTS AND DISCUSSION

Shown in the main panels of Fig. 2(a) and 2(c) are a representative set of $G(V)$ curves at T up to 10 K, far beyond the superconducting resistive transition temperature $T_c^{\text{onset}} \simeq 3.4\text{ K}$ for samples A and B, respectively. As shown, the $G(V)$ curves exhibit several common characteristics: At low T 's, $G(V)$ spectra display dips at zero bias, and double shoulders at around 0.43 mV and double kinks around 1.0 mV, as marked by the black and red arrows, respectively. The double-shoulder and double-kink features are considered telltale signatures of two-band superconductivity [38,40]. Moreover, a dip, instead of a sharp peak at zero bias, excludes the possibility of a nodal gap in CsV_3Sb_5 .

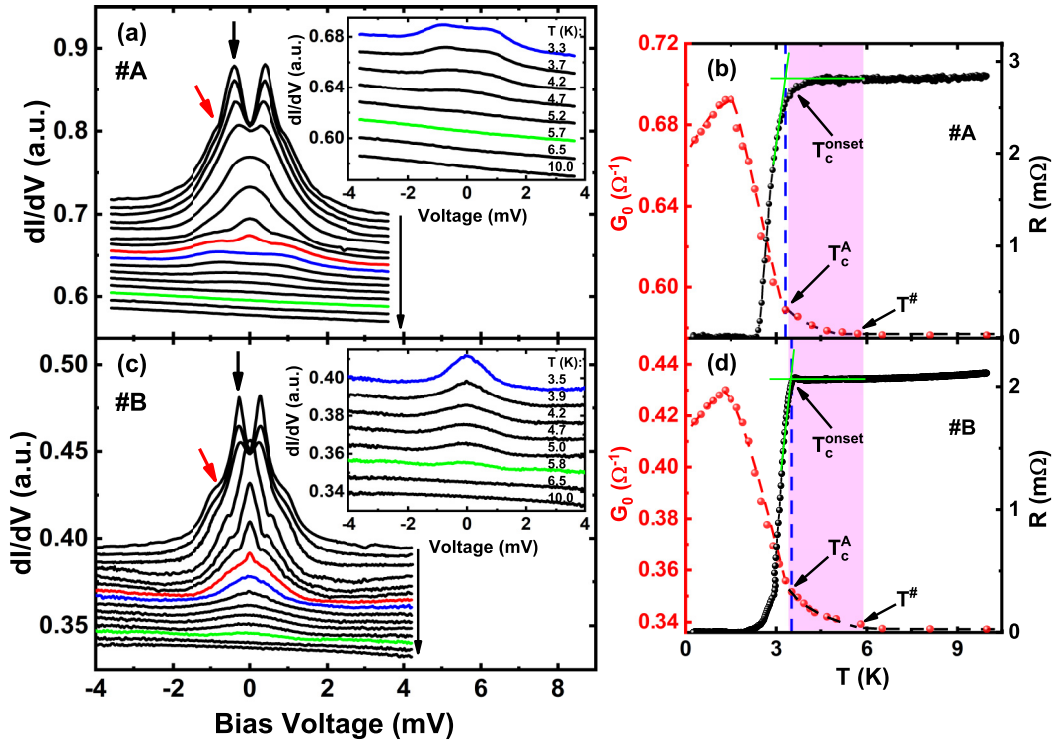


FIG. 2. (a), (c) Raw data of soft point-contact conductance spectrum $G(V) \equiv dI/dV$ vs bias voltage V at various T 's from 0.3 K to 10.0 K for samples A and B, respectively. The $G(V)$ curves are vertically shifted for clarity except the one at the highest T . The insets are the enlarged view of SPCS at $T > T_c$. (b), (d) The corresponding zero bias conductance G_0 and resistance R in the superconducting transition regime both as a function of T for a comparison. The dashed red and black lines in (b) and (d) are guides to the eye, and the vertical blue dashed lines in (b) and (d) represent the temperatures of 3.3 K and 3.5 K, respectively. The colored shadows in (b) and (d) mark the G_0 -tail region between T_c^A and $T^\#$.

With increasing T , an unexpected feature becomes apparent in these $G(V)$ curves when the overall magnitude of the Andreev conductance is gradually suppressed: As T approaches the onset of the superconducting transition $T_c^{\text{onset}} \simeq 3.4$ K, the Andreev spectrum does not immediately reach bias-independent unity. Instead, as shown in the inset of Fig. 2(a), at 3.3 K, significant spectral conductance remains below about 1.0 mV with approximately 6% of Andreev intensity remaining at zero bias (blue curve). The excess $G(V)$ gradually decreases, becoming essentially featureless at $T^\# \simeq 5.7$ K (green curve). With further increase of T , the $G(V)$ spectrum evolves into a T -independent, antisymmetric linear curve with a slight slope. The excess spectral conductance in the high T range manifests itself as an enhancement of the zero-bias conductance G_0 above the normal state G_N . As shown in Fig. 2(b), G_0 shows a “tail” with a clear inflection point at T_c^A , the gap opening/closing temperature. Here, for sample A, $T_c^A \simeq 3.3$ K almost coincides with T_c^{onset} , the upper superconducting resistive transition temperature, which rules out the existence of a pseudogap state in CsV_3Sb_5 [41]. Similar evolution of $G(V)$ in T , including the excess $G(V)$ and G_0 tail above T_c^A , is observed for sample B with $T_c^A \simeq 3.5$ K and $T^\# \simeq 5.8$ K, as shown in Figs. 2(c) and 2(d). Very recently, the same behaviors of point-contact $G(V)$ spectra have been observed in both CsV_3Sb_5 and KV_3Sb_5 crystals [42].

The observed excess spectral conductance in the normal state could be considered as fingerprints of the unconventional density of state (DOS) energy distribution in the vicinity of

the Fermi level. Theoretically, there is not presently a comprehensive model that fully accounts for the origin of the excess spectral conductance above T_c . Phenomenologically, for weakly correlated superconductors, such as PbTaSe_2 [34,35], PdBi_2 [43], and $(\text{Y,Lu})\text{Ni}_2\text{B}_2\text{C}$ [44], there is no excess $G(V)$ above T_c . In contrast, for strongly electron-correlated systems such as iron pnictides [45] and heavy-fermion superconductors [46,47], excess $G(V)$ above T_c is ubiquitous and is ascribed to electronic correlation effects [45,46,48]. We surmise that the presence of such broad excess $G(V)$ above T_c and the resulting tail feature with positive curvature in CsV_3Sb_5 are an indicator of modest electron-electron correlations in such stoichiometric kagome metals.

To explicitly describe the variety of spectral behaviors observed and quantitatively extract the gap amplitude, we invoke a generalized 2D Blonder-Tinkham-Klapwijk (BTK) model [49] with two s -wave conductance channels: $G(V) = \varpi G^L(V) + (1 - \varpi)G^S(V)$, where ϖ quantifies the relative spectral weight of the two channels. In the 2D BTK model [50], the Andreev conductance spectrum $G(V)$ can be expressed with three parameters: a dimensionless parameter Z which represents the interface transparency, an imaginary quasiparticle energy term Γ (Dynes factor) which describes the spectral broadening, and the superconducting energy gap Δ . As shown in the main panel of Fig. 3(a), the two-channel 2D BTK model provides an excellent description of the normalized $G(V)$ at the lowest $T = 0.3$ K. The best fits yields $\Delta^L = 1.05$ meV, $\Gamma^L = 0.24$ meV, and $Z^L = 0.68$, for the

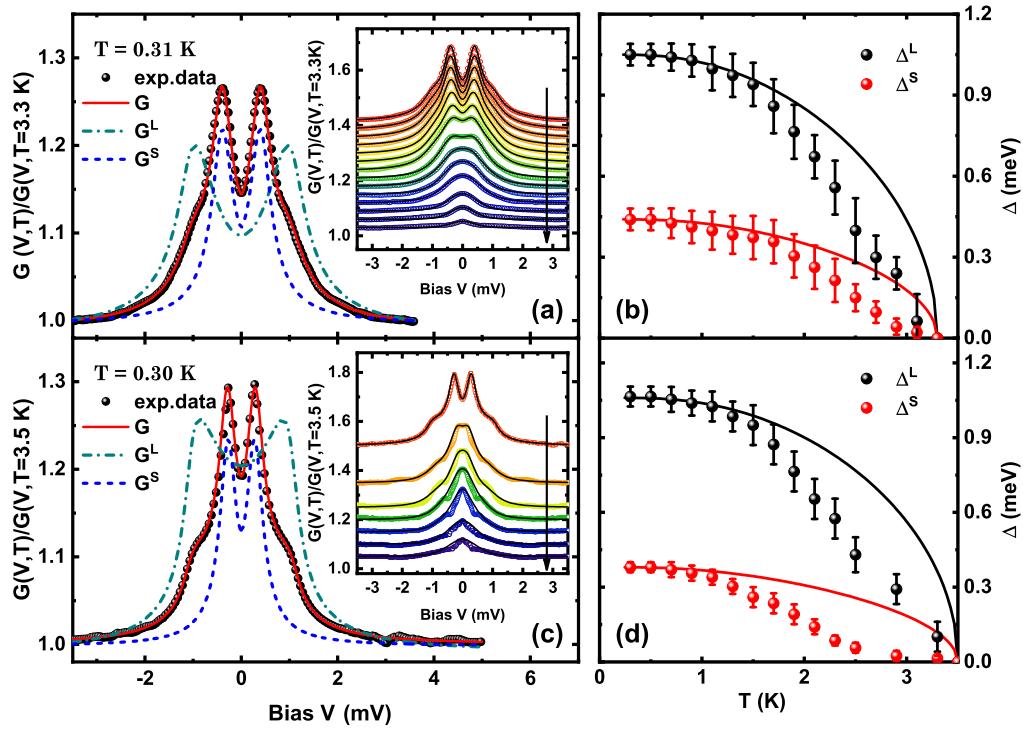


FIG. 3. Normalized conductance spectrum $G(V)/G(V, T_c^A)$ for samples (a) A and (c) B at the lowest measurement T , and fittings based on the generalized 2D BTK model. The total conductance spectral $G(V)$ (solid red lines) is the summary of the partial conductance spectral G^L and G^S with the weight ϖ , i.e., $G(V) = \varpi G^L(V) + (1 - \varpi)G^S(V)$. Insets: Temperature evolution of the normalized conductance curves from 0.3 K to 2.9 K and their fits by 2D BTK model with the fixed ϖ . (b), (d) Temperature evolution of the extracted energy gaps Δ^L and Δ^S for samples A and B, respectively. The colored solid lines are the BCS Δ - T fitting lines.

large-gap channel, and $\Delta^S \simeq 0.45$ meV, $\Delta^S = 0.14$ meV, and $Z^S = 0.63$ for the small-gap channel. The spectral weight for the larger gap is around 27%, indicating a predominance of the small-gap channel. The reliability of the analysis is further evidenced by similar results obtained from applying the same procedure to the sample B Andreev junction. The fittings are shown in the main panel of Fig. 3(c), which yield $\Delta^L = 1.06$ meV, $\Gamma^L = 0.12$ meV, $Z^L = 0.86$, and $\Delta^S = 0.38$ meV, $\Gamma^S = 0.12$ meV, $Z^S = 0.73$, and a spectral weight $\varpi \simeq 24\%$. Here, the results, including the gap values and spectral weight, are highly consistent with those obtained from a similar soft PCS of CsV_3Sb_5 crystal [42]. Furthermore, the obtained gap values in CsV_3Sb_5 quantitatively agree with the prediction of a two-band electron-phonon coupling model, which sets boundaries for the two superconducting gaps [51], $\Delta^L > \Delta_{\text{BCS}} \simeq 0.52$ meV $>$ Δ^S , as observed in the canonical two-gap superconductor MgB_2 [52].

Based on the best-fit parameters obtained above, we extend the analysis to all conductance spectra measured at temperatures below T_c . As shown in the insets of Figs. 3(a) and 3(c), the two-gap 2D BTK model provides good fits to all $G(V)$ curves. In all fittings, ϖ is kept constant for each sample, while Γ increases slightly with T up to T_c . The resulting gaps Δ^L and Δ^S for samples A and B are plotted as functions of T , shown in Figs. 3(b) and 3(d), respectively. The obtained gaps can be approximated by an empirical BCS formula: $\Delta(T) = \Delta_0 \tanh(\alpha\sqrt{T_c/T} - 1)$ where α is adjustable parameter [53]. For sample A, $\Delta_0^L = 1.05$ meV, $\Delta_0^S = 0.455$ meV. Here, T_c as

fitting parameters are equivalent to T_c^A of samples A and B, as expected.

We now discuss the implications of our results on the nature of superconductivity in the kagome superconductor CsV_3Sb_5 . While the small gap of $\Delta^S \simeq 0.45$ meV coincides with one of those obtained by STM and μSR experiments [30,54,55], the gap $\Delta^L \simeq 1.0$ meV is quite large in magnitude comparing with those reported from bulk nature measurements such as muon spin rotation/relaxation (μSR) [55] and specific heat experiments [29]. For example, μSR measurements of the magnetic penetration depth exhibit an $(s + s)$ -wave gap symmetry with the larger gap of 0.57 meV and $T_c \simeq 2.5$ K [55]. One might argue that the larger gap of PCS measurement originates from surface state superconductivity as nontrivial topological surface states have been reported in these kagome compounds [11,56], and the gap value for the topological surface superconductivity could be different from the bulk counterpart [57,58]. However, in general, PCS is a bulk spectroscopic probe, and the probing depth is estimated to be about $2\text{--}3 \xi$ (ξ is the superconducting coherence length) into the sample surface [59]. Using $\mu_0 H_{c2}^{//ab} = \frac{\phi_0}{2\pi \xi_c^2}$, where $\mu_0 H_{c2}^{//ab}$ is the upper critical field ($\mu_0 H_{c2}^{//ab} \simeq 7.2$ T for CsV_3Sb_5 [60]) and $\phi_0 = 2.07 \times 10^{-15}$ Wb the flux quantum, the probing length for ARS measurement is estimated to be about $\sim 4\text{--}7$ nm, confirming the bulk nature of the point-contact spectroscopy measurement. Moreover, the surface-sensitive STM experiment identified a larger

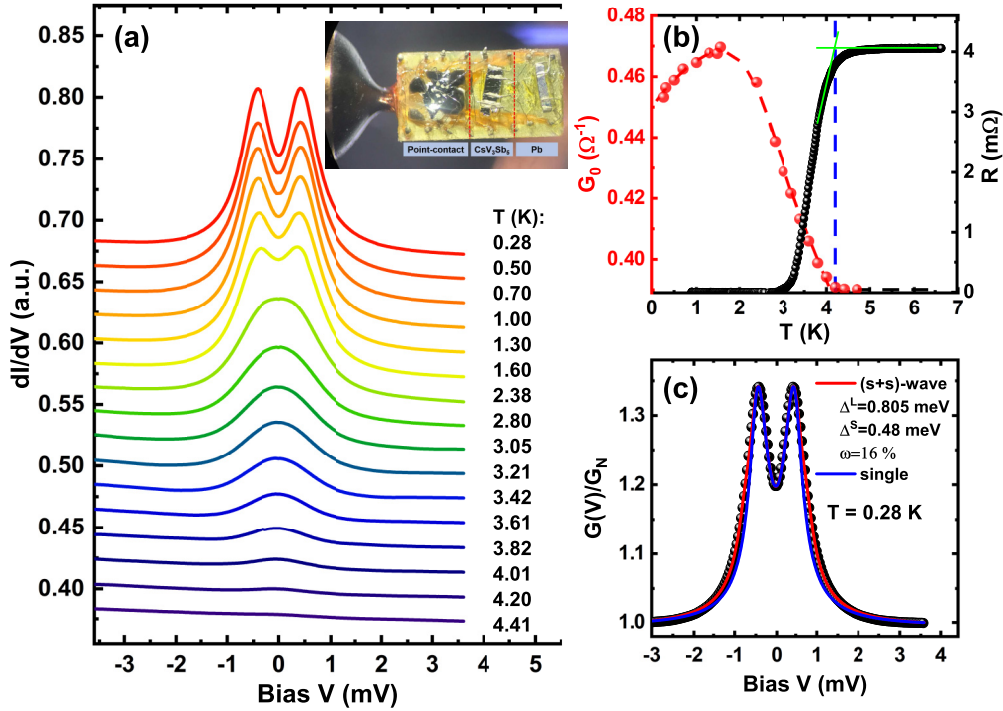


FIG. 4. Conductance spectra and resistance of a bulk sample of A both under a hydrostatic pressure. (a) Raw differential conductance curves $G(V)$ of a $\text{Ag}/\text{CsV}_3\text{Sb}_5$ (sample A) point-contact junction at various T 's under a quasihydrostatic pressure of 2.1 kbar. The conductance spectrum $G(V)$ is vertically shifted for clarity except the one at the highest T . Inset: The measuring configuration for pressure-dependent point-contact spectroscopy. (b) The corresponding zero-bias conductance G_0 and resistance R of a bulk sample A in the superconducting transition regime both as a function of T for a comparison. The red and black dashed lines are guides to the eye, with the vertical blue dashed lines representing the temperature of 4.2 K. (c) The normalized conductance spectral $G(V)/G_N$ at the lowest T and its fits to two s -wave gap (red solid curve). A single s -wave gap BTK fit is also plotted (blue solid curve) for comparison.

superconducting gap of 0.56 meV [30], fully consistent with the bulk gap probed by μSR experiment. The consistency between the surface-sensitive and bulk gaps imposes a constraint on the existence of surface superconductivity of CsV_3Sb_5 .

Instead, we interpret the gap ratio $2\Delta_0^L/k_B T_c^A \simeq 7.2$ as an indicator of a strong coupling strength for CsV_3Sb_5 . This value of coupling strength is much larger than those of typical two-gap superconductor MgB_2 (~ 4.16) [32], topological superconductor PbTaSe_2 (~ 3.70) [34,35], and typical CDW superconductors 2H-NbSe_2 ($\simeq 3.59$) and TaS_2 ($\simeq 3.85$) [61,62]; on the other hand, the coupling strength is close to those of iron-based superconductors, such as LiFeAs [63,64], KFe_2As_2 (~ 7.2) [65], in which there exists a van Hove singularity in the electronic density of states in the vicinity of the Fermi level E_F . In the framework of the conventional BCS theory, the superconducting gap is expressed as $\Delta_{\text{sc}} \sim e^{-1/\lambda}$, where λ is a product of $N(0)$, the DOS at the Fermi level, and V_i the pairing interaction mediated by exchanging bosons [66]. In the scenario of electron-phonon coupling, a strong-coupling strength implies a large DOS at E_F .

The high DOS at E_F of CsV_3Sb_5 mainly arises from one or more flat-band-associated VHSs at the Fermi level. According to the first-principles electronic structure calculations [21,67], the kagome bands can host two different types of VHSs at the M point in the Brillouin zone. Specifically, for CsV_3Sb_5 , the calculations demonstrate that a van Hove singularity (VHS1) with the orbital content of $V d_{x^2-y^2}$, d_{z^2} , and d_{xy} in character is located at ~ 50 meV, and VHS2 with d_{xz} , d_{yz} character

is located at ~ 100 meV from E_F . Several angle-resolved photoemission spectroscopy (ARPES) studies have identified these twofold VHSs near the Fermi level of CsV_3Sb_5 , including both VHS1- and VHS2-type kagome bands. Among these VHSs, the VHS2 is located closer to the Fermi level and is characterized by sharp Fermi surface nesting [68,69]. As a consequence, the saddle points of VHSs lead to a logarithmic divergence of the DOS at E_F , thus suggesting the predominance of a high DOS for Cooper pairing in strong-coupling strength. It is interesting to note that in magic-angle twisted bilayer graphene, a honeycomb lattice which resembles the kagome lattice, its superconductivity has been associated with the high DOS of its flat bands [70].

To gain further insight into the impact of the van Hove singularity on the superconductivity of CsV_3Sb_5 , we performed T -dependent point-contact ARS combined with resistivity measurements on sample A under a hydrostatic pressure of 2.1 kbar [34]. As shown in the inset of Fig. 4(a), a $\text{CsV}_3\text{Sb}_5/\text{Ag}$ point-contact junction together with a piece of CsV_3Sb_5 control sample was fed into a BeCu piston-cylinder cell (PCC) in which a quasihydrostatic pressure was generated by mechanically pressing Daphne 7373. The pressure values in PCC were determined from the change of superconducting transition temperature of Pb, ΔT_c^{Pb} . Shown in Fig. 4(a) is a set of conductance spectra at various T 's for the Andreev junction. The conductance curves show a double-shoulder feature at 0.45 mV at low T 's, which is nearly in agreement with that at ambient pressure. The most notable difference, however, is

that the kink feature in $G(V)$ is substantially weakened under such pressure. Moreover, concomitant with the suppression of the large gap feature, the broad excess $G(V)$ at $T > T_c^A$ fades away. Alternatively, the absence of excess $G(V)$ is evident in the T dependence of the zero-bias conductance G_0 , as shown in Fig. 4(b). Instead, under p , G_0 goes to a T -independent constant smoothly at an enhanced $T_c^A \simeq 4.2$ K, in accord with a similarly enhanced superconducting resistive transition temperature T_c^{onset} by pressure.

We quantitatively analyze the measured Andreev reflection spectrum at $T = 0.28$ K by the aforementioned BTK fitting procedure. Notably, as shown in Fig. 4(c), the two s -wave gap model provides a noticeably better description of the data than the one based on a single s -wave gap, indicating the persistence of the two nodeless superconducting gaps under the pressure. The best two-gap BTK fit yields $\Delta^L = 0.81$ meV and $\Delta^S = 0.48$ meV, and a somewhat diminished spectral weight of $\varpi^L = 16\%$ for the larger gap. Remarkably, the extracted small gap Δ^S almost remains essentially unchanged from that at ambient p , while both the amplitude and the spectral weight of the larger gap Δ^L are reduced upon applied p . Our observations seem to be consistent with those of a metal-tip locally pressurized CsV_3Sb_5 point contact, in which case the larger gap and its spectral weight disappeared under a large local pressure or strain [42]. Band structure calculations show that under external p both VHS1 and VHS2 experience a shift with respect to the Fermi level, manifesting as the saddle points moving linearly away from the Fermi level [67,71,72]. As the van Hove singularities located at the M point move away from the Fermi level, they may induce a decrease in $N(0)$, and lead to the reduction of both the larger gap and its spectral weight contributing to superconductivity. On the other hand, the $V-d_{z^2}$ -related van Hove singularity located at the Γ point is supposed to move closer to the Fermi level under pressure, accompanied by an increase in the $N(0)$ [72].

To elucidate the role of the DOS $N(0)$ at the Fermi level on the kagome superconductivity CsV_3Sb_5 , we define a spectral-weighted superconducting gap $\Delta_{\text{ave}} = \varpi \Delta^L + (1 - \varpi) \Delta^S$ as a measure of the overall superconducting DOS at E_F and examine its relation with the multigap superconductivity. At $p = 2.1$ kbar, $\Delta_{\text{ave}} \simeq 0.533$ meV and $T_c^A \simeq 4.2$ K, leading to a weighted gap ratio $\frac{2\Delta_{\text{ave}}}{k_B T_c^A} \simeq 2.94$. For a comparison, at ambient pressure $\Delta_{\text{ave}} \simeq 0.62$ meV with $T_c^A \simeq 3.3$ K, leading to a gap ratio of 4.36. The reduced coupling strength leads to a reduced total DOS for the superconducting state upon pressure. In the scenario of the electron-phonon strong-coupling mechanism, the reduced total superconducting DOS at the Fermi level cannot account for the enhanced T_c upon the hydrostatic pressure.

In line with the argument that the excess $G(V)$ and the resulting positive curvature G_0 tail are the consequences of electronic correlation, our observation of the disappearance of excess $G(V)$ and G_0 tail under applied pressure indicate the electronic correlation is effectively suppressed by the pressure, leading to an enhancement of T_c^{onset} and T_c^A . Considering magnetic effects such as magnetic fluctuations and/or the V $3d$ orbital order, Zhang *et al.* performed the DFT+ U calculations to examine the electronic correlation effect and the possible magnetism on the vanadium atoms [73]. With

a small U value, a ferrimagnetic state with a nonzero net magnetic moment in the unit cell is found to be a more stable phase than those of the nonmagnetic state at ambient pressure. In this scenario, the hydrostatic pressure can be understood to effectively suppress the ferrimagnetism on the vanadium atoms and drive the system to a nonmagnetic state, and as a consequence restoring conventional superconductivity with an enhanced T_c . Therefore, although the kagome flat band and its associated VHSs have been considered an essential ingredient in the electronic structure of CsV_3Sb_5 relevant for the superconductivity, the role of the V $3d$ inherent magnetism cannot be disregarded [73], particularly for such magnetically frustrated kagome system.

Finally, we offer a general discussion on the interplay between the CDW order and superconductivity in CsV_3Sb_5 under the relatively low p . Under this pressure, the CDW transition occurs at $T_{\text{CDW}} \simeq 81.5$ K, as indicated by a resistivity anomaly [22,23]. Increasing pressure leads to a suppression to the CDW, but no significant changes to the band structure in the normal state. In a Bilbro-McMillan partial gapping scenario, the CDW competes strongly with superconductivity at the Fermi surface [74]. Under this p , the CDW deformation strongly decreases the DOS at the Fermi energy by suppressing the van Hove singularities [72]. As a consequence, a decreasing T_{CDW} indicates a reduced DOS due to the CDW order. As for the superconducting state, applying pressure decreases the total DOS for superconducting pairing. The situation contradicts the expected partial gapping scenario in the model of CDW-superconductivity competition, similarly to the case of $2H\text{-NbSe}_2$ in which the superconducting state is only weakly dependent on the pressure-modulated CDW state [75]. Future spectroscopy experiments should examine systematically the evolution of flat-band-associated VHSs and the relation between superconducting and CDW orders, together with the precise understanding of the magnetism of the V atoms under varying pressures.

IV. CONCLUSIONS

We have performed soft point-contact Andreev reflection spectroscopy combined with resistivity measurements on single crystals of the kagome superconductor CsV_3Sb_5 , in order to ascertain its superconducting coupling strength (gap size Δ and T_c). The distinct soft PCS spectra at low temperatures evidence multigap superconductivity under ambient and low pressure. The observation of a pronounced large superconducting gap together with an excess spectral conductance spectrum above T_c , and their suppression by a hydrostatic pressure, points to the importance of both a strong-coupling mechanism and electron correlations for the kagome superconductivity in CsV_3Sb_5 at ambient pressure. Taken together, the results suggest that pairing in CsV_3Sb_5 is likely to be conventional multigap in nature, but is partially suppressed by the magnetism on the vanadium atoms.

ACKNOWLEDGMENTS

C.R. expresses gratitude to Professor Hai-hu Wen for insightful discussions. This work is supported by the National

Natural Science Foundation of China (Grants No. 11774303, No. 11574373, No. 12074002, and No. 11974246). C.R. acknowledges financial support from the Joint Fund of Yunnan Provincial Science and Technology Department (Grant No. 2019FY003008). X.Y.H. acknowledges financial support by the National Natural Science Foundation of China (Grant No. 11804379). H.C.L. was supported by the National Key R&D

Program of China (Grant No. 2018YFE0202600) and Beijing Natural Science Foundation (Grant No. Z200005), Beijing National Laboratory for Condensed Matter Physics. Y.Q. would like to acknowledge the National Key R&D Program of China (Grant No. 2018YFA0704300), and P.X. acknowledges financial support by National Science Foundation Grant No. DMR-1905843.

- [1] M. R. Norman, *Rev. Mod. Phys.* **88**, 041002 (2016).
- [2] Y. Shimizu, K. Miyagawa, K. Kanoda, M. Maesato, and G. Saito, *Phys. Rev. Lett.* **91**, 107001 (2003).
- [3] M. P. Shores, E. A. Nytko, B. M. Bartlett, and D. G. Nocera, *J. Am. Chem. Soc.* **127**, 13462 (2005).
- [4] A. O'Brien, F. Pollmann, and P. Fulde, *Phys. Rev. B* **81**, 235115 (2010).
- [5] F. Pollmann, K. Roychowdhury, C. Hotta, and K. Penc, *Phys. Rev. B* **90**, 035118 (2014).
- [6] W.-S. Wang, Z.-Z. Li, Y.-Y. Xiang, and Q.-H. Wang, *Phys. Rev. B* **87**, 115135 (2013).
- [7] S. V. Isakov, S. Wessel, R. G. Melko, K. Sengupta, and Y. B. Kim, *Phys. Rev. Lett.* **97**, 147202 (2006).
- [8] F. H. Yu, D. H. Ma, W. Z. Zhuo, S. Q. Liu, X. K. Wen, B. Lei, J. J. Ying, and X. H. Chen, *Nat. Commun.* **12**, 3645 (2021).
- [9] S.-L. Yu and J.-X. Li, *Phys. Rev. B* **85**, 144402 (2012).
- [10] B. R. Ortiz, L. C. Gomes, J. R. Morey, M. Winiarski, M. Bordelon, J. S. Mangum, I. W. H. Oswald, J. A. Rodriguez-Rivera, J. R. Neilson, S. D. Wilson, E. Ertekin, T. M. McQueen, and E. S. Toberer, *Phys. Rev. Mater.* **3**, 094407 (2019).
- [11] B. R. Ortiz, S. M. L. Teicher, Y. Hu, J. L. Zuo, P. M. Sarte, E. C. Schueller, A. M. M. Abeykoon, M. J. Krogstad, S. Rosenkranz, R. Osbron, R. Seshadri, L. Balent, J. He, and S. D. Wilson, *Phys. Rev. Lett.* **125**, 247002 (2020).
- [12] B. R. Ortiz, P. M. Sarte, E. M. Kenney, M. J. Graf, S. M. L. Teicher, R. Seshadri, and S. D. Wilson, *Phys. Rev. Mater.* **5**, 034801 (2021).
- [13] N. Shumiya, M. S. Hossain, J. X. Yin, Y. X. Jiang, B. R. Ortiz, H. Liu, Y. Shi, Q. Yin, H. Lei, S. S. Zhang, G. Chang, Q. Zhang, T. A. Cochran, D. Multer, M. Litskevich, Z. J. Cheng, X. P. Yang, Z. Guguchia, S. D. Wilson, and M. Z. Hasan, *Phys. Rev. B* **104**, 035131 (2021).
- [14] F. H. Yu, T. Wu, Z. Y. Wang, B. Lei, W. Z. Zhuo, J. J. Ying, and X. H. Chen, *Phys. Rev. B* **104**, L041103 (2021).
- [15] S.-Y. Yang, Y. Wang, B. R. Ortiz, D. Liu, J. Gayles, E. Derunova, R. Gonzalez-Hernandez, L. Smejkal, Y. Chen, S. S. P. Parkin, S. D. Wilson, E. S. Toberer, T. McQueen, and M. N. Ali, *Sci. Adv.* **6**, eabb6003 (2020).
- [16] J. Zhao, W. Wu, Y. Wang, and S. A. Yang, *Phys. Rev. B* **103**, L241117 (2021).
- [17] H. Tan, Y. Liu, Z. Wang, and B. Yan, *Phys. Rev. Lett.* **127**, 046401 (2021).
- [18] E. M. Kenney, B. R. Ortiz, C. Wang, S. D. Wilson, and M. J. Graf, *J. Phys.: Condens. Matter* **33**, 235801 (2021).
- [19] M. L. Kiesel and R. Thomale, *Phys. Rev. B* **86**, 121105(R) (2012).
- [20] L. H. C. M. Nunes and C. Morais Smith, *Phys. Rev. B* **101**, 224514 (2020).
- [21] X. Wu, T. Schwemmer, T. Müller, A. Consiglio, G. Sangiovanni, D. Di Sante, Y. Iqbal, W. Hanke, A. P. Schnyder, M. Michael Denner, M. H. Fischer, T. Neupert, and R. Thomale, *Phys. Rev. Lett.* **127**, 177001 (2021).
- [22] K. Y. Chen, N. N. Wang, Q. W. Yin, Z. J. Tu, C. S. Gong, J. P. Sun, H. C. Lei, Y. Uwatoko, and J.-G. Cheng, *Phys. Rev. Lett.* **126**, 247001 (2021).
- [23] X. Chen, X. Zhan, X. Wang, J. Deng, Xiao-bing Liu, X. Chen, Jian-gang Guo, and X. Chen, *Chin. Phys. Lett.* **38**, 057402 (2021).
- [24] B. Q. Song, X. M. Kong, W. Xia, Q. W. Yin, C. P. Tu, C. C. Zhao, D. Z. Dai, K. Meng, Z. C. Tao, Z. J. Tu, C. S. Gong, H. C. Lei, Y. F. Guo, X. F. Yang, and S. Y. Li, [arXiv:2105.09248](https://arxiv.org/abs/2105.09248).
- [25] Y. Wang, S.-Y. Yang, P. K. Sivakumar, B. R. Ortiz, S. M. L. Teicher, H. Wu, A. K. Srivastava, C. Garg, D. Liu, S. S. P. Parkin, E. S. Toberer, T. McQueen, S. D. Wilson, and M. N. Ali, [arXiv:2012.05898](https://arxiv.org/abs/2012.05898).
- [26] C. C. Zhao, L. S. Wang, W. Xia, Q. W. Yin, J. M. Ni, Y. Y. Huang, C. P. Tu, Z. C. Tao, Z. J. Tu, C. S. Gong, H. C. Lei, Y. F. Guo, X. F. Yang, and S. Y. Li, [arXiv:2102.08356](https://arxiv.org/abs/2102.08356).
- [27] C. Mu, Q. Yin, Z. Tu, C. Gong, H. Lei, Z. Li, and J. Luo, *Chin. Phys. Lett.* **38**, 077402 (2021).
- [28] J. Luo, Z. Zhao, Y. Z. Zhou, J. Yang, A. F. Fang, H. T. Yang, H. J. Gao, R. Zhou, and Guo-qing Zheng, *npj Quantum Mater.* **7**, 30 (2022).
- [29] W. Duan, Z. Nie, S. Luo, F. Yu, B. R. Ortiz, L. Yin, H. Su, F. Du, A. Wang, Y. Chen, X. Lu, J. Ying, S. D. Wilson, X. Chen, Y. Song, and H. Yuan, *Sci. China Phys. Mech. Astron.* **64**, 107462 (2021).
- [30] H.-S. Xu, Y.-J. Yan, R. Yin, W. Xia, S. Fang, Z. Chen, Y. Li, W. Yang, Y. Guo, and D.-L. Feng, *Phys. Rev. Lett.* **127**, 187004 (2021).
- [31] Y. Fu, N. Zhao, Z. Chen, Q. Yin, Z. Tu, C. Gong, C. Xi, X. Zhu, Y. Sun, K. Liu, and H. Lei, *Phys. Rev. Lett.* **127**, 207002 (2021).
- [32] P. Szabó, P. Samuely, J. Kačmarčík, T. Klein, J. Marcus, D. Fruchart, S. Miragha, C. Marcenat, and A. G. M. Jansen, *Phys. Rev. Lett.* **87**, 137005 (2001).
- [33] S. Sasaki, M. Kriener, K. Segawa, K. Yada, Y. Tanaka, M. Sato, and Y. Ando, *Phys. Rev. Lett.* **107**, 217001 (2011).
- [34] H. Zi, L.-X. Zhao, X.-Y. Hou, L. Shan, Z. Ren, G.-F. Chen, and C. Ren, *Chin. Phys. Lett.* **37**, 097403 (2020).
- [35] T. Le, Y. Sun, H.-K. Jin, L. Che, L. Yin, J. Li, G. M. Pang, C. Q. Xu, L. X. Zhao, S. Kittaka, T. Sakakibara, K. Machida, R. Sankar, H. Q. Yuan, G. F. Chen, X. Xu, S. Li, Y. Zhou, and X. Lu, *Sci. Bull.* **65**, 1349 (2020).
- [36] T. Y. Chen, Z. Tesanovic, R. H. Liu, X. H. Chen, and C. L. Chien, *Nature (London)* **453**, 1224 (2008).
- [37] D. Daghero, M. Tortello, G. A. Ummarino, and R. S. Gonnelli, *Rep. Prog. Phys.* **74**, 124509 (2011).

- [38] R. S. Gonnelli, D. Daghero, G. A. Ummarino, V. A. Stepanov, J. Jun, S. M. Kazakov, and J. Karpinski, *Phys. Rev. Lett.* **89**, 247004 (2002).
- [39] Y. Naidyuk, O. Kvitnitskaya, D. Bashlakov, S. Aswartham, I. Morozov, I. Chernyavskii, G. Fuchs, S.-L. Drechsler, R. Hühne, K. Nielsch, B. Büchner, and D. Efremov, *2D Mater.* **5**, 045014 (2018).
- [40] Z. Hol'ánová, P. Szabó, P. Samuely, R. H. T. Wilke, S. L. Bud'ko, and P. C. Canfield, *Phys. Rev. B* **70**, 064520 (2004).
- [41] H. Chen, H. Yang, B. Hu, Z. Zhao, J. Yuan, Y. Xing, G. Qian, Z. Huang, G. Li, Y. Ye, Q. Yin, C. Gong, Z. Tu, H. Lei, S. Ma, H. Zhang, S. Ni, H. Tan, C. Shen, X. Dong *et al.*, *Nature (London)* **599**, 222 (2021).
- [42] L. Yin, D. Zhang, C. Chen, G. Ye, F. Yu, B. R. Ortiz, S. Luo, W. Duan, H. Su, J. Ying, S. D. Wilson, X. Chen, H. Yuan, Y. Song, and X. Lu, *Phys. Rev. B* **104**, 174507 (2021).
- [43] L. Che, T. Le, C. Q. Xu, X. Z. Xing, Z. Shi, X. Xu, and X. Lu, *Phys. Rev. B* **94**, 024519 (2016).
- [44] X. Lu, W. K. Park, S. Yeo, K.-H. Oh, S.-I. Lee, S. L. Bud'ko, P. C. Canfield, and L. H. Greene, *Phys. Rev. B* **83**, 104519 (2011).
- [45] D. Daghero and R. S. Gonnelli, *Supercond. Sci. Technol.* **23**, 043001 (2010).
- [46] W. K. Park, J. L. Sarrao, J. D. Thompson, and L. H. Greene, *Phys. Rev. Lett.* **100**, 177001 (2008).
- [47] G. Goll, H. v. Löhneysen, I. K. Yanson, L. Taillefer, *Phys. Rev. Lett.* **70**, 2008 (1993).
- [48] M. Fogelström, W. K. Park, L. H. Greene, G. Goll, and M. J. Graf, *Phys. Rev. B* **82**, 014527 (2010).
- [49] G. E. Blonder, M. Tinkham, and T. M. Klapwijk, *Phys. Rev. B* **25**, 4515 (1982).
- [50] S. Kashiwaya, Y. Tanaka, M. Koyanagi, and K. Kajimura, *Phys. Rev. B* **53**, 2667 (1996).
- [51] V. G. Kogan, C. Martin, and R. Prozorov, *Phys. Rev. B* **80**, 014507 (2009).
- [52] H. J. Choi, D. Roundy, H. Sun, M. L. Cohen, and S. G. Louie, *Nature (London)* **418**, 758 (2002).
- [53] H. Padamsee, J. E. Neighbor, and C. A. Shiffman, *J. Low Temp. Phys.* **12**, 387 (1973).
- [54] Z. Liang, X. Hou, F. Zhang, W. Ma, P. Wu, Z. Zhang, F. Yu, J.-J. Ying, K. Jiang, L. Shan, Z. Wang, and X.-H. Chen, *Phys. Rev. X* **11**, 031026 (2021).
- [55] R. Gupta, D. Das, C. H. Mielke III, Z. Guguchia, T. Shiroka, C. Baines, M. Bartkowiak, H. Luetkens, R. Khasanov, Q. Yin, Z. Tu, C. Gong, and H. Lei, *npj Quantum Mater.* **7**, 49 (2022).
- [56] Y. Hu, S. M. L. Teicher, B. R. Ortiz, Y. Luo, S. Peng, L. Huai, J. Z. Ma, N. C. Plumb, S. D. Wilson, J.-F. He, and M. Shi, *Sci. Bull.* **67**, 495 (2022).
- [57] W. Liu, L. Cao, S. Zhu, L. Kong, G. Wang, M. Papaj, P. Zhang, Y.-B. Liu, H. Chen, G. Li, F. Yang, T. Kondo, S. Du, G.-H. Cao, S. Shin, L. Fu, Z. Yin, H.-J. Gao, and H. Ding, *Nat. Commun.* **11**, 5688 (2020).
- [58] S. Y. Guan, P. J. Chen, M. W. Chu, R. Sankar, F. Chou, H. T. Jeng, C. S. Chang, and T. M. Chuang, *Sci. Adv.* **2**, e1600894 (2016).
- [59] Yu. G. Naidyuk and I. K. Yanson, *Point-Contact Spectroscopy*, Springer Series in Solid-State Sciences (Springer, 2005).
- [60] S. Ni, S. Ma, Y. Zhang, J. Yuan, H. Yang, Z. Lu, N. Wang, J. Sun, Z. Zhao, D. Li, S. Liu, H. Zhang, H. Chen, K. Jin, J. Cheng, L. Yu, F. Zhou, X. Dong, J. Hu, H.-J. Gao *et al.*, *Chin. Phys. Lett.* **38**, 057403 (2021).
- [61] X.-Y. Hou, F. Zhang, X.-H. Tu, Y.-D. Gu, M.-D. Zhang, J. Gong, Y.-B. Tu, B.-T. Wang, Wen-Gang Lv, H.-M. Weng, Z.-A. Ren, G.-F. Chen, X.-D. Zhu, N. Hao, and L. Shan, *Phys. Rev. Lett.* **124**, 106403 (2020).
- [62] J. A. Galvis, L. Chirulli, I. Guillamon, S. Vieira, E. Navarro-Moratalla, E. Coronado, H. Suderow, and F. Guinea, *Phys. Rev. B* **89**, 224512 (2014).
- [63] T. Hänke, S. Sykora, R. Schlegel, D. Baumann, L. Harnagea, S. Wurmehl, M. Daghofer, B. Büchner, J. van den Brink, and C. Hess, *Phys. Rev. Lett.* **108**, 127001 (2012).
- [64] S. V. Borisenko, V. B. Zabolotnyy, D. V. Evtushinsky, T. K. Kim, I. V. Morozov, A. N. Yaresko, A. A. Kordyuk, G. Behr, A. Vasiliev, R. Follath, and B. Büchner, *Phys. Rev. Lett.* **105**, 067002 (2010).
- [65] D. Fang, X. Shi, Z. Du, P. Richard, H. Yang, X. X. Wu, P. Zhang, T. Qian, X. Ding, Z. Wang, T. K. Kim, M. Hoesch, A. Wang, X. Chen, Jiangping Hu, H. Ding, and H.-H. Wen, *Phys. Rev. B* **92**, 144513 (2015).
- [66] M. Tinkham, *Introduction to Superconductivity*, 2nd ed. (McGraw-Hill Book Co., New York, 2004).
- [67] H. LaBollita and A. S. Botana, *Phys. Rev. B* **104**, 205129 (2021).
- [68] M. Kang, S. Fang, J.-K. Kim, B. R. Ortiz, S. H. Ryu, J. Kim, Jonggyu Yoo, G. Sangiovanni, D. Di Sante, B.-G. Park, C. Jozwiak, A. Bostwick, E. Rotenberg, E. Kaxiras, S. D. Wilson, J.-H. Park, and R. Comin, *Nat. Phys.* **18**, 301 (2022).
- [69] K. Nakayama, Y. Li, T. Kato, M. Liu, Z. Wang, T. Takahashi, Y. Yao, and T. Sato, *Phys. Rev. B* **104**, L161112 (2021).
- [70] M. Oh, K. P. Nuckolls, D. Wong, R. L. Lee, X. Liu, K. Watanabe, T. Taniguchi, and A. Yazdani, *Nature (London)* **600**, 240 (2021).
- [71] A. A. Tsirlin, P. Fertey, B. R. Ortiz, B. Klis, V. Merkl, M. Dressel, S. D. Wilson, and E. Uykur, *SciPost Phys.* **12**, 049 (2022).
- [72] J.-G. Si, W.-J. Lu, Y.-P. Sun, P.-F. Liu, and B.-T. Wang, *Phys. Rev. B* **105**, 024517 (2022).
- [73] J.-F. Zhang, K. Liu, and Z.-Y. Lu, *Phys. Rev. B* **104**, 195130 (2021).
- [74] G. Bilbro and W. L. McMillan, *Phys. Rev. B* **14**, 1887 (1976).
- [75] Y. Feng, J. Wang, R. Jaramillo, J. van Wezel, S. Haravifard, G. Srajer, Y. Liu, Z. A. Xu, P. B. Littlewood, and T. F. Rosenbaum, *Proc. Natl. Acad. Sci. USA* **109**, 7224 (2012).